Wiley Online Library
Early View publication on www.wileyonlinelibrary.com
(issue and page numbers not yet assigned;
citable using Digital Object Identifier – DOI)

J. Biophotonics 1–10 (2016) / **DOI** 10.1002/jbio.201600007

Journal of BIOPHOTONICS

FULL ARTICLE

A novel multiphoton microscopy images segmentation method based on superpixel and watershed

*Weilin Wu***[1,2], *Jinyong Lin***[3], *Shu Wang*[1,2], *Yan Li*[1,2], *Mingyu Liu*[1,2], *Gaoqiang Liu*[1,2], *Jianyong Cai*[1,2], *Guannan Chen**[1,2], *and Rong Chen*[1,2]

[1] Key Laboratory of OptoElectronic Science and Technology for Medicine of Ministry of Education Fujian Normal University, Fuzhou, Fujian, 350007, China
[2] Department of Network and Communication Engineering, Fujian Normal University, Fuzhou, Fujian, 350007, China
[3] Department of Radiation Oncology, Fujian Provincial Cancer Hospital, Fuzhou, Fujian 350014, China

Received 11 January 2016, revised 24 March 2016, accepted 28 March 2016
Published online 20 April 2016

Key words: multiphoton microscopy, phase congruency feature, superpixels, watershed, image segmentation

Multiphoton microscopy (MPM) imaging technique based on two-photon excited fluorescence (TPEF) and second harmonic generation (SHG) shows fantastic performance for biological imaging. The automatic segmentation of cellular architectural properties for biomedical diagnosis based on MPM images is still a challenging issue. A novel multiphoton microscopy images segmentation method based on superpixels and watershed (MSW) is presented here to provide good segmentation results for MPM images. The proposed method uses SLIC superpixels instead of pixels to analyze MPM images for the first time. The superpixels segmentation based on a new distance metric combined with spatial, CIE Lab color space and phase congruency features, divides the images into patches which keep the details of the cell boundaries. Then the superpixels are used to reconstruct new images by defining an average value of superpixels as image pixels intensity level. Finally, the marker-controlled watershed is utilized to segment the cell boundaries from the reconstructed images. Experimental results show that cellular boundaries can be extracted from MPM images by MSW with higher accuracy and robustness.

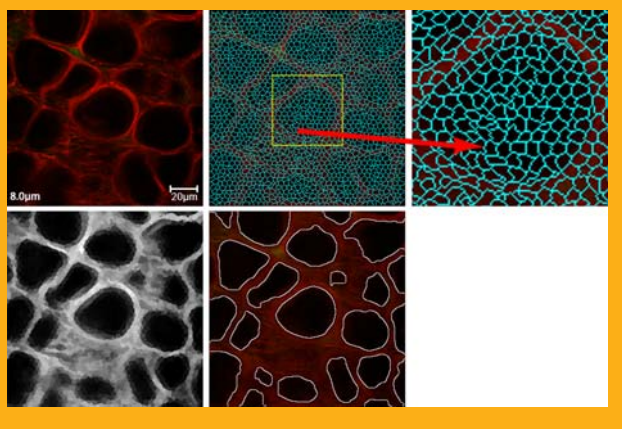

1. Introduction

Multiphoton Microscopy is considered as an effective biological imaging technique, which has been widely used for exploring the structure and dynamic interactions of tissues and was first demonstrated in a biological application proposed by Denk et al. [1] in 1990. Compared with other visualizing techniques, such as magnetic resonance imaging (MRI) [2], optical coherence tomography (OCT) [3] and positron emission tomography (PET) [4], the MPM has many unique advantages, including reduced specimen photo-bleaching, enhanced penetration depth, and high resolution without adding exogenous fluoro-

* Corresponding author: e-mail: edado@fjnu.edu.cn
** Weilin Wu and Jinyong Lin are co-first authors; they contributed equally to the work.

Journal of BIOPHOTONICS

phores into cellular and sub-cellular microstructure of biological tissue. The MPM imaging technique relies on two-photon exicted fluorescence (TPEF) and second harmonic generation (SHG) signals of biological tissues and a combination of the two mechanisms can supply complementary information on structure and function of tissue. The new challenges for clinical applications (e.g. histological analyses) of this imaging technology are the automatic segmentation of cellular architectural properties on the MPM images.

Image segmentation plays an important role in biological image analysis for getting important information (objects' size, shape, area, positions, and other meaningful properties) [5]. The segmentation results for MPM images are usually not satisfactory due to the influence of several factors, such as intensity inhomogeneous in different depth, low signal to noise ratio (SNR) and blurring cellular boundaries [6, 7] (Figure 1). So far, the most effective ways for cell segmentation in nonlinear optical images (i.e., MPM) are watershed-based and level-set-methods (LSM) based algorithms [8–11]. The watershed-based algorithms [11–14] have strong robustness in recognizing cells with heavily viscous status in uniform-illuminated images. However, the details of the image for the cell boundary are still imprecise, facing over-segmentation problem. Another approach to segment MPM image is based on LSM, which integrates whole image features. This method could resist the influence of the noise and distinguish multiple targets from the background simultaneously [9, 15–17]. But the details of the image of viscous cell whose boundary is fuzzy still couldn't be recognized exactly. Other methods such as multi-featured detecting method [7], statistical pixel intensity model [5], graph-cuts [18], hidden-Markov models [19] and three-step hierarchical method [10] were published. Although some of these approaches have a good performance, most of them were time-consuming, complex and need initial parameters.

This paper proposes a novel automatic cell segmentation algorithm based on superpixels and watershed method for MPM images to delineate cell boundaries. The structure of this paper is as follows: specimens preparation and image acquisition are introduced in Section 2. Section 3 reviews the SLIC superpixels technique and illustrates a novel distance measure and the proposed MSW method for cell segmentation. Experimental results and discussion are presented in Section 4. And the paper is concluded in Section 5.

2. Specimens preparation and image acquisition

2.1 Animal models and specimens preparation

In this study, the biopsy samples were obtained from ten ears of five adult New Zealand white rabbits, and each ear of the rabbits received two punch wounds of 8 mm diameter from the medial surface extending deep through the cartilage without penetrating the lateral skin. A biopsy sample was collected from the margin of the wound of each rabbit using a 2 mm diameter biopsy punch. The experimental procedures were endorsed by the Fujian Medical University and approval of the Animal Care and Use committee (Fujian Medical University) with ethics permissions.

2.2 MPM images acquisition

MPM system was performed on a commercial LSM 510 META (Zeiss, Inc.) coupled to a mode-locked Ti: sapphire laser operating at 810 nm (Mira 900-F; Coherent, Inc.). A Plan-Neofluar objective (×40, N. A. 0.75, Zeiss, Inc.) was used in all experiments for focusing the excitation beam (average power less than 5 mW) into the repairing tissue samples and was also applied to collect the backscattered intrinsic SHG/TPEF signals. Two independent channels of the META detector were employed to capture the high-contrast SHG and TPEF images from the specimen: one channel covered the wavelength range from 430–697 nm for collecting TPEF signals, another channel covered the wavelength range from 398–409 nm for collecting SHG signals. For obtaining large-area images, an optional HRZ 200 fine fo-

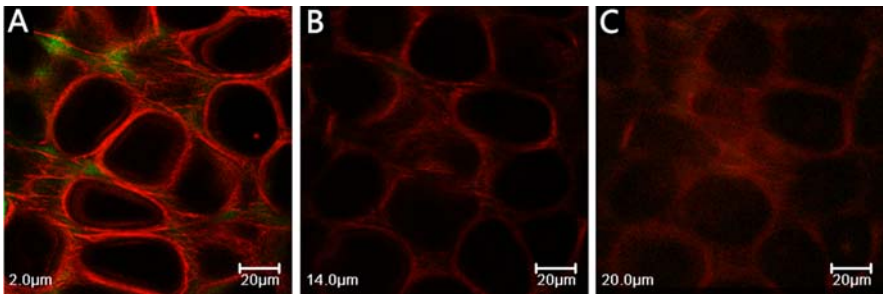

Figure 1 Example of three MPM images at various depths from elastic cartilage of rabbit ears: (**A**) 2 μm, (**B**) 14.0 μm, (**C**) 20.0 μm. TPEF images (red) are extracted from 430 nm to 697 nm, while SHG images (green) were extracted from 398 nm to 409 nm. And the excitation wavelength was 810 nm.

cusing stage (Carl Zeiss) was applied to translate the motorized x–y scanning stage. Additionally, by changing the focal plane (Z-level) to image at various depths, the obtained images (12 sequential 2D images at depth intervals of 2 μm, the maximum depth was up to 22 μm) were used for quantitative analysis. All images (512×512 pixels) were obtained at 2.56 μs and 6.4 μm per pixel and each pixel has a 12-bit depth.

3. Image processing

3.1 Superpixel technique

A superpixel is a perceptually meaningful patch of pixels with same or similar properties (i.e., local intensity, position). For an image, superpixels segmentation is capable of achieving a good performance by enhancing cell identification and segmentation, especially in the images of close cell positions, with uneven background as well as low SNR. In this section, the foundations of the original simple linear iterative clustering (SLIC) superpixels algorithm and a novel distance metric are explained.

3.1.1 Superpixel segmentation algorithm

Recently, superpixels algorithms [20–23] have been widely used as a crucial preprocessing stage for image segmentation. The SLIC-based method has shown a great performance in superior boundary recall, high computing efficiency, as well as low under-segmentation error. SLIC algorithm [23] adapts k-means clustering method to create superpixels by weighting the 5-D space $\{L, a, b, x, y\}$, where L, a, b are the values of the CIE Lab color space and x, y represent pixels spatial coordinates. SLIC defined the parameter K as desired number of superpixels. Then for a color images in CIE Lab color space with N pixels, the similar size of each superpixels is N/K. For approximately sized superpixels, the grid interval $S = \sqrt{N/K}$ was set as the superpixels center. The euclidean distance metric D_s determined the nearest cluster for each pixel, which is defined in Eq. (1). Then, each pixel is allocated to the nearest clustering center. When each pixel has been allocated to the nearest cluster center, the cluster center is updated and controlled by the mean LABXY vector of all the pixels belonging to the cluster. Finally, update steps will reassign disjoint pixels to nearby superpixels.

$$D_s = \sqrt{\mathrm{Dist}_c^2 + \left(\frac{\mathrm{Dist}_{xy}}{S}\right)^2 m^2} \quad (1)$$

where Dist_c is the color distance in CIE Lab color space and Dist_{xy} represents x–y plane distance, which is represented at Section 3.2. Variable m is defined to compact the superpixels.

3.1.2 Distance measure

In SLIC, the distance metric with some properties was required to generate compact superpixels. Due to the inhomogeneous intensity, low SNR and blurring cellular boundaries, it was difficult to isolate the cell from background. We propose a novel distance measure with three terms for generating highly similar superpixels, which are color, spatial position and phase congruency (PC) distance. Figure 2 shows the details of the proposed new distance measure for SLIC. At initialization step, seeds are selected on a regular grid spaced Spixels apart, which are the center of grid and set as initial superpixels cluster centers $C_k = [L_k, a_k, b_k, x_k, y_k, pc_k]^T$. For each superpixel, the similarity of the i^{th} pixel and k^{th} seed, is computed by the proposed new distance D is defined in Eq. (2). Each pixel is allocated to the nearest clustering center. Then update task is executed to adjust the cluster centers according to the mean $[L, a, b, x, y, pc]^T$ vector of all the pixels belonging to the cluster. Finally, the steps of the SLIC super-

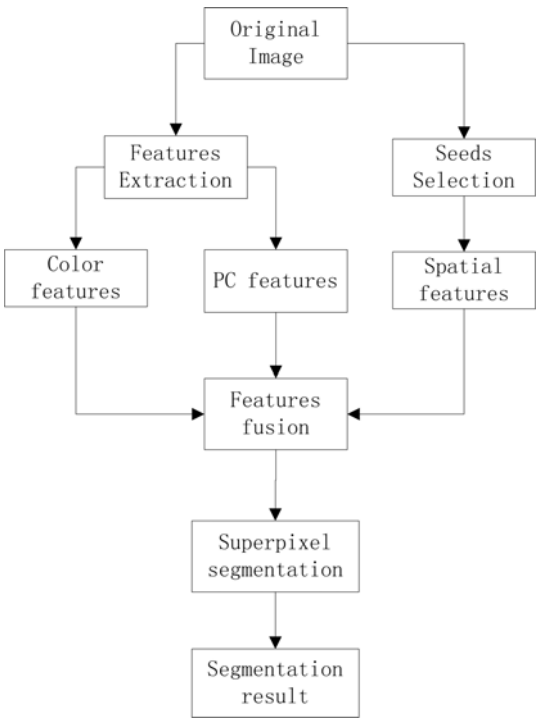

Figure 2 Proposed new distance for SLIC superpixels segmentation.

pixels segmentation method are updated to obtain good segmentation results.

$$D = \mathrm{e}^{\left(\frac{\mathrm{Dist}_c}{\varsigma}\right)} + \frac{\mathrm{Dist}_{xy}}{S^2 m^2} + \frac{\mathrm{Dist}_{\mathrm{PC}}}{\xi} \tag{2}$$

By defining D in this way, ς, m, and ξ are weights of each properties which allows us to assign the relative importance among color similarity, spatial proximity and PC features. When ς is small, the superpixels segmentation results are greatly influenced by color similarity. When ς is large, the superpixels segmentation results are determined by spatial proximity or PC features. ς value can be set in the range (0,1). When the variable m is large, spatial proximity is more vital and the superpixels are more compact. When m is small, superpixels segmentation results are more tightly adhered to the image boundaries with less regular shape and size. While the CIE LAB color space is used in this model, m value can be set in the range (1,40). When the ξ is large, color similarity is more important and the superpixels has poor boundary adherence where the object boundary is fuzzy. When the variable ξ is small, the segmentation is mainly based on PC features and spatial similarity that results superpixels is more tightly adhered to the fuzzy boundaries of the objects. And the ξ value can be set in range (0,1).

In the first term, Dist_c tis the CIE Lab color distance (Eq. (3)) and this term can depress the internal color of the superpixels to be uniform. The second term is a search restriction for compact superpixels, and Dist_{xy} is the spatial position distance. The final term is a boundary condition, and $\mathrm{Dist}_{\mathrm{PC}}$ is the PC distance.

$$\mathrm{Dist}_c = \sqrt{(L_k - L_i)^2 + (a_k - a_i)^2 + (b_k - b_i)^2} \tag{3}$$

$$\mathrm{Dist}_{xy} = \sqrt{(x_k - x_i)^2 + (y_k - y_i)^2} \tag{4}$$

$$\mathrm{Dist}_{\mathrm{PC}} = \mathrm{PC}(k) - \mathrm{PC}(i) \tag{5}$$

where l, a, b are the color values in the CIE Lab color space and x, y are the spatial position. PC is the phase congruency features which is introduced in Section 3.1.3. And Dist_{xy} and $\mathrm{Dist}_{\mathrm{PC}}$ are necessary to be normalized in the range from 0 to 1. The maximum values for normalization is the maximum values of the local region.

3.1.3 Phase congruency

Phase congruency (PC) [24] method is a vital feature detection operator in the field of image processing. There are two main advantages of this operator. It can detect a wide range of features from images and remains unchanged against the local intensity of the images change. When the intensity and contrast changed, the feature detection results of the phase congruency method basically keep steady without adjusting any parameters. PC is redefined as follows:

$$\mathrm{PC}(x) = \frac{\sum_u W(x)\, \|A_u(x)\, \Delta\Phi_u(x) - T\|}{\sum_u A_u + \varepsilon} \tag{6}$$

where $W(x)$ is the weighted function which can devalue phase congruency at the location where the spread of frequency response is narrow and is defined at Eq. (7). A_u represents the magnitude of the u^{th} of Fourier component. $\Delta\Phi_u(x)$ is deviation of phase. $\|\cdot\|$ denotes that the enclosed quantity is equal to itself when its value is positive, and zero otherwise. T is the estimated noise, and ε is a very small positive real number and set to be equal to 0.0001.

$$W(x) = \frac{1}{1 + \mathrm{e}^{\mu(c - s(x))}} \tag{7}$$

where μ is a factor which is used to control the sharpness of the cutoff, $c$is a constant and $s(x)$ represents the frequency response spread.

$$s(x) = \frac{1}{U}\left(\frac{\sum_u A_u(x)}{A_{\max}(x) + \varepsilon}\right) \tag{8}$$

Where U is the total number of the Fourier components being used and $A_{\max}(x)$ is $A_u(x)$ which has the maximum response at position x.

$$\Delta\Phi_u(x) = \cos\left(\Phi_u(x) - \bar{\Phi}(x)\right) - |\sin\left(\Phi_u(x) - \bar{\Phi}(x)\right)| \tag{9}$$

Where $\Phi_u(x)$ is defined as the local phase of the Fourier component. And $\bar{\Phi}(x)$ is the average of the local phase angles.

3.2 Segmentation using superpixel and watershed

The segmentation method for multiphoton microscopy image using superpixels and watershed (MSW) is presented, which makes full use of the advantages of the MSW method for automatic delineation of cells from MPM images with low SNR, blur-

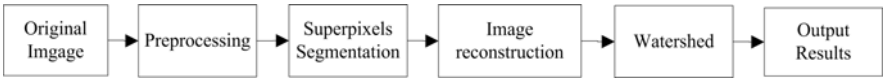

Figure 3 Flowchart of the proposed MSW segmentation.

ring cell boundaries and inhomogeneous intensity problems. The flowchart of the algorithm is described in Figure 3. The details of steps are as follows:

Step 1. Preprocess the original MPM image (512×512 pixels) with histogram equalization and Gaussian filtering with $\sigma = 1$.

Step 2. Rough Segmentation of the images by SLIC superpixels algorithm according to the new distance metric (Eq. (2)) in terms of the colors (Eq. (3)), spatial (Eq. (4)) and phase congruency (Eqs. (5) and (6)) distribution.

Step 3. Reconstruction of the new image by treating each superpixel as a unit, and set $\mathrm{Gray}_{i,k} = \sqrt{(\bar{l}_k{}^2 + \bar{a}_k{}^2 + \bar{b}_k{}^2)}$ as each pixel's value ($\bar{l}$, $\bar{a}$, $\bar{b}$ are the average color values of the superpixel in the CIE Lab space. k is the k^{th} superpixel, i represents as the i^{th} pixel of the k^{th} superpixel).

Step 4. Process the reconstructed image by Gaussian filter. Employ the marker-controlled watershed [25] to delineate the cell boundaries from the new image. Use the extended maxima operator to identify groups of pixels which are significantly higher than proximal region. Modify the image to force the extended maxima pixels to be the local minima [26] in the image. The markers are the local minima of the gradient of the image. Finally, compute the watershed transform.

4. Results and discussion

In order to verify the validity of our algorithm, several experiments were performed on the MPM images. Three normal and two regenerated elastic cartilage specimens at 20-week repair time points were measured with MPM at various depths (in total 60 images, each group 12 sequences), and one group of the images is shown in Figure 1. The proposed algorithm was implemented in the MATLAB 2013a programming environment and run on a personal computer with 2.5 GHz Core CPU and 4 GB RAM.

In this paper, the number of superpixels K is set to be 2000 for each image, the values of ς, m, ξ in Eq. (2) are set to be 0.09,15 and 0.09, respectively. The radius parameter of Gaussian filter in the Step 4 is set to be 10, the sigma parameter is half of the radius. The height parameter for the extended maxima operator in the marker-controlled watershed is set to 8.

4.1 Experimental results of the proposed algorithm

Segmentation results of elastic cartilage tissue MPM image are displayed in Figure 4. As shown in Figure 4(a), the original MPM image shows low SNR, and the boundaries between cells and tissues around

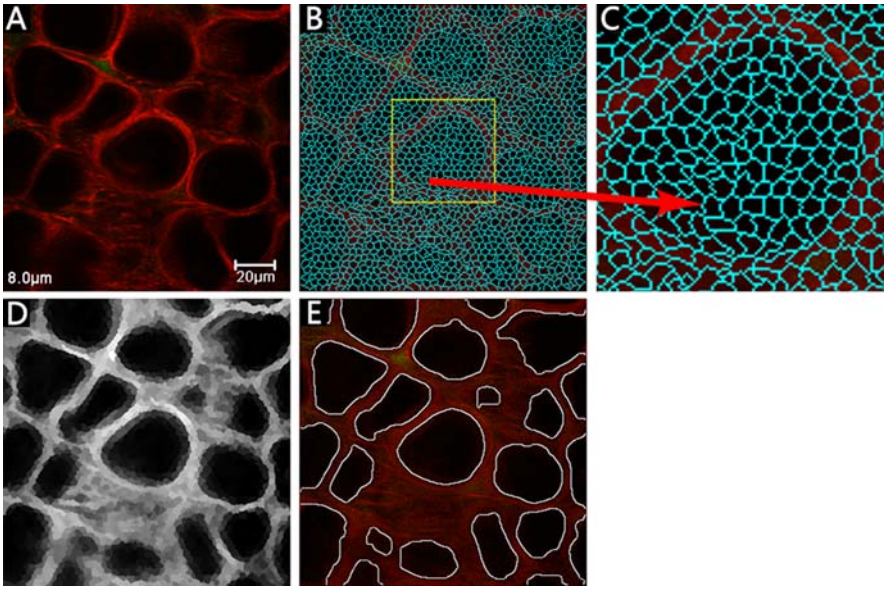

Figure 4 Segmentation results of rabbit elastic cartilage MPM image at depth $Z = 8$ μm. (**A**) the original image; (**B**) the segmentation results of SLIC algorithm with the proposed new distance measure; (**C**) the details of the superpixels segmentation result; (**D**) the reconstruction based on superpixels; (**E**) segmentation result. The blue and white curves represent the superpixels and cells boundaries, respectively.

are not clear-cut enough to be accurately located by human eyes. The results of the superpixels segmentation based on SLIC algorithm with new distance measure are shown in Figure 4(b). In Figure 4(c), it can be seen that the information of the boundaries are saved in the superpixels, which is significant for next reconstruction step. Noises are depressed and boundaries are enhanced after the reconstruction in Figure 4(d). Finally, the proposed MSW algorithm can exactly delineate the cells from the complex background in Figure 4(e).

4.2 Comparison with other methods

In this section, we compared the MSW method with two well-known methods (the watershed based and LSM based segmentation algorithms). The Watershed and LSM algorithms are commonly used segmentation methods in nonlinear optical imaging images [6, 8–11, 17, 25, 27]. In order to perform a fair comparison, we set the same pre-processing step for both pixel-based watershed and LSM method, and superpixel-based MSW method to process the images.

Figure 5 shows the segmentation results of the three algorithms performed on four MPM image sets. Obviously, the proposed MSW method attained the best result which has more intact cell contour and more smooth boundary than the other two methods. Especially for the normal samples at 16 μm depth where the original MPM images show intensity inhomogeneity with serious noise impact, the traditional watershed and LSM method get the improper segmentation results, whereas the proposed MSW method still obtain satisfactory cell boundary in the image.

For further illustrates, the proposed MSW method has a fantastic performance in processing MPM images. The detailed segmentation results of two MPM images from a normal elastic cartilage and a wound healing one are analyzed. From Figures 6–7, we found that the white contour of our method get closer to the real cell boundary than the other two approaches while the Watershed and the LSM method exit serious over-segmentation and under-segmentation phenomenon. Although there are some inhomogeneous intensity area in the MPM images which is shown in Figure 7 D1 and D4 regions, the MSW performed very well, while the Watershed and the Level-Set gets the error boundary.

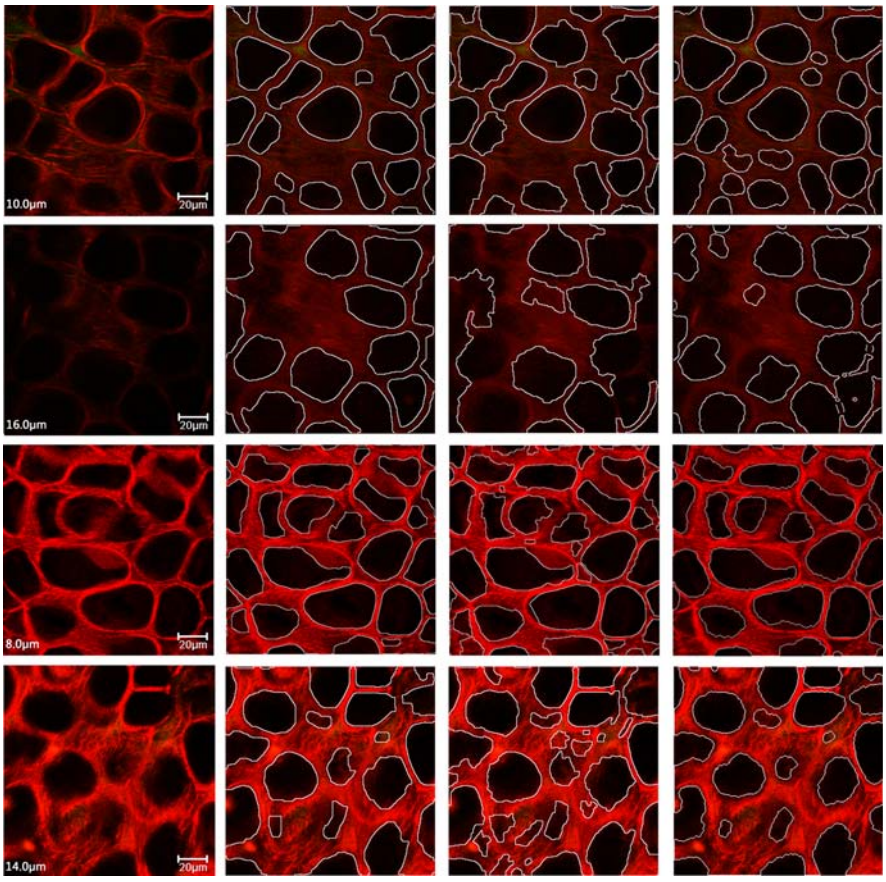

Figure 5 Representative MPM images in order are from two normal samples at depth $Z = 10$ μm, 16 μm respectively and two regenerated elastic cartilage specimens after 20-week repair at depth $Z = 8$ μm, 14 μm separately. Comparisons between the proposed algorithm and classical algorithm. First column: the original MPM images; second column: segmentation results by the proposed; third column: segmentation results of the watershed method; last column: segmentation results of the LSM.

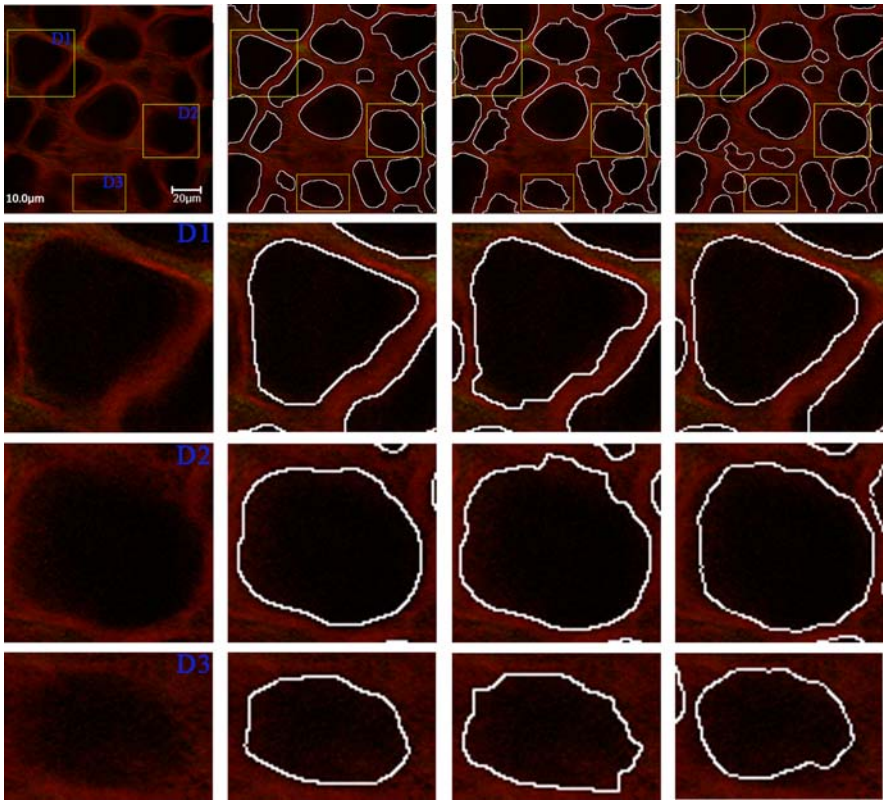

Figure 6 Representative MPM images from an intact elastic cartilage at depth $Z = 10$ μm shows details of segmentation results by comparing the proposed MSW method, the watershed and the LSM approach. The 1st column is the original MPM images which is in the 5th 2 μm in MPM image sets of normal elastic cartilage; the 2nd column get the segmention results by the proposed MSW; the 3rd column is the results of the Watershed; the last column obtain the results from the LSM. D1–D3 are the details of the first line.

Besides subjective comparison, we also achieve quantitative verification. In order to evaluate the performance of our proposed approach, we compute and compare the automatic segmentation results with a so-called ground truth, which is manually segmented [10]. And the metrics are calculated by three scores: accuracy, specificity and sensitivity, which are defined by

$$\text{Accuracy} = \frac{\text{TP} + \text{TN}}{\text{TP} + \text{FN} + \text{TN} + \text{FP}} \tag{10}$$

$$\text{Sensitivity} = \frac{\text{TP}}{\text{TP} + \text{FN}} \tag{11}$$

$$\text{Specificity} = \frac{\text{TN}}{\text{TN} + \text{FP}} \tag{12}$$

where TP, TN, FP and FN are marked as true positives, true negatives, false positives and false negatives, respectively. Additionally, for verifying that our method is robust in different depths which have different intensity, a total of 60 MPM images are set as three groups: top, middle and bottom group (Top, middle and bottom groups represent MPM images at 0–8 μm, 9–16 μm and 17–24 μm depths, respectively).

The above-described metrics method for the cell segmentation are implemented; i.e., the Watershed method, the LSM, and the proposed method are used for comparison, the validation of the segmentation results are described in Table 1. The proposed segmentation method has higher segmentation accuracy than the classical Watershed and LSM algorithms. Meanwhile, compared with MSW which uses a classical distance measure, the proposed method with new distance measure shows higher performance in accuracy, sensitivity and specificity. The average of CPU times consumed by the proposed method for 60 images is 31.5 s, and the corresponding CPU time consumed by watershed, LSM and MSW_C are 1.4 s, 28.3 s and 30.2 s, respectively.

4.3 Discussion

The MPM images have low SNR, blurring cell boundaries, and intensity inhomogeneity problems. The traditional algorithms had some limitations on processing MPM images. For example, they were sensitive to noise and required a high contrast between objects and background. The watershed-based algorithm was a simulation that was based on relief flooding model to find the watershed line. It could isolate viscous cell from complex background and had high robustness in inhomogeneous intensity. However, the method used morphological operation

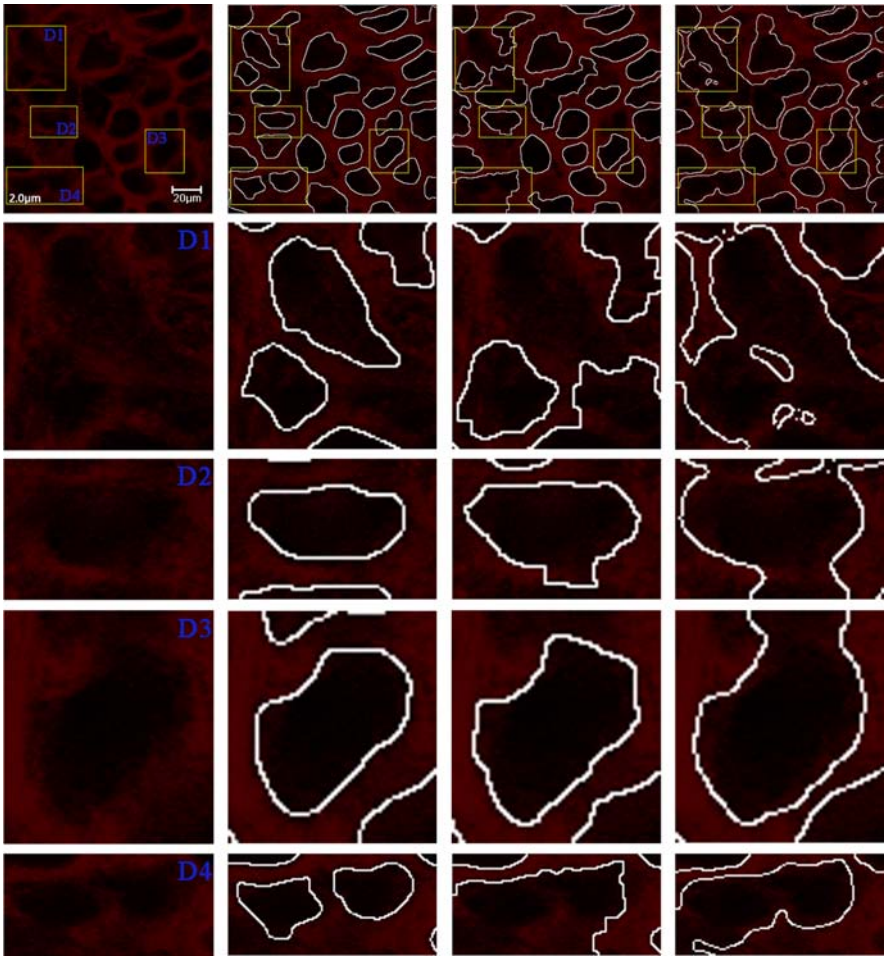

Figure 7 Details comparison of Segmentation results by the proposed MSW method, the watershed and the LSM method. The 1st column is the original images which is representative MPM images from an regenerated elastic cartilage at depth $Z = 2$ μm; second column get the segmentation results by the proposed MSW; third column is the results of the Watershed; the last column obtain the results from the LSM. The D1–D4 is the details of the first line.

to smooth the image, leading to a decrease of useful information and poor segmentation results in cell periphery. The LSM approach was evolving a contour to isolate regions from initial boundary with the global and local features. It had a good performance in eliminating influence of noise and low contrast. But results of viscous cell were debased, and the globally optimal result was unguaranteed.

Therefore, we proposed a novel method based on superpixels and watershed approach to segment the MPM images. Superpixels technique is used in MPM images segmentation for the first time with taking advantage of spatial constraint information and increasing the granularity of the clustering. A new distance metric is utilized for controlling and generating superpixels, which consists of spatial, CIE Lab color space and phase congruency features. Phase congruency is frequency features that supply much clear-cut edge information, so the proposed MSW have a good performance in keeping the details of the cell boundaries and avoiding the influences of noise, inhomogeneous intensity as well as fuzzy cellular boundaries. Then the original image is reconstructed and each pixels of image is replaced with the average value of superpixels. Finally, the cell boundaries are segmented from the recon-

Table 1 Comparison of the segmentation accuracy (sensitivity/specificity) of cell segmentation methods (%).

Group	Watershed	LSM	MSWC	Proposed
Top*	89.5(93.0/85.9)	84.8(76.3/93.2)	95.4(95.3/95.5)	**96.5**(96.5/96.4)
Middle*	89.1(93.1/89.4)	86.0(80.0/92.3)	94.7(94.1/95.2)	**95.7**(95.3/96.0)
Bottom*	85.1(86.0/84.1)	80.2(68.5/95.3)	94.1(92.6/95.7)	**95.7**(94.6/97.0)
Total	88.2(91.2/85.0)	84.0(75.5/93.4)	94.1(94.2/95.4)	**96.0**(95.6/96.4)

* Top, middle and bottom groups represent MPM images at 0–8 μm, 9–16 μm and 17–24 μm depths, respectively. Abbreviation: MSW_C, MSW with a classical distance measure.

Table 2 CPU times consuming of automatical segmentation methods (s).

Size	Watershed	LSM	MSW_C	MSW
512 × 512	1.4	28.3	30.2	31.5

structed MPM images with the marker-controlled watershed method. MSW effectively utilizes both advantages of SLIC superpixels and watershed methods by combing them in MPM images analysis, and consider global and local features of image. Therefore, we demonstrate an optimized algorithm, which has perfect performance in delineating the cells from MPM images, with better details of the cell boundaries and higher robustness.

5. Conclusion

In this paper, the superpixels segmentation method was employed for MPM images analysis for the first time. The MSW method segments the cell boundary automatically and is motivated by both SLIC superpixels and the marker-based watershed method. Firstly, a novel distance metric with spatial and CIE Lab color space and phase congruency features was utilized to improve the superpixels segmentation. Then the image was reconstructed based on superpixels for the next processing. Finally, the marked-controlled watershed method was employed to isolate cells from complex background. The proposed method has been tested for MPM images of elastic cartilage tissue with a great improvement for intensity inhomogeneity, blurred cell boundaries, viscous cell and low SNR problem. On the basis of that, we envision that the MSW method would potentially serve as an effective segmentation method for MPM images.

Acknowledgements This work was supported in main by the program for Changjiang Scholars and Innovative Research Team in University (No. IRT_15R10), and the National Natural Science Foundation of China (No. 81101110, No. 61210016) and the Science and Technology Project of Fujian Province (No. 2015J01300).

Author biographies Please see Supporting Information online.

References

[1] W. Denk, J. H. Strickler, and W. W. Webb, Science **248**, 73–76 (1990).
[2] D. Le Bihan, Magnetic Resonance Quarterly **7**, 1–30 (1991).
[3] J. F. De Boer, B. Cense, B. H. Park, M. C. Pierce, G. J. Tearney, and B. E. Bouma, Optics Letters **28**, 2067–2069 (2003).
[4] G. Muehllehner and J. S. Karp, Physics in Medicine and Biology **51**, R117 (2006).
[5] A. Calapez and A. Rosa, Image Processing, IEEE Transactions on **19**, 2408–2418 (2010).
[6] K. Mkrtchyan, D. Singh, M. Liu, V. Reddy, A. Roy-Chowdhury, and M. Gopi, Image Processing (ICIP), 2011 18th IEEE International Conference (2011), pp. 2165–2168.
[7] A. Medyukhina, T. Meyer, M. Schmitt, B. F. Romeike, B. Dietzek, and J. Popp, Journal of Biophotonics **5**, 878–888 (2012).
[8] E. Meijering, Signal Processing Magazine, IEEE **29**, 140–145 (2012).
[9] M. Liu, A. Chakraborty, D. Singh, R. K. Yadav, G. Meenakshisundaram, G. V. Reddy, and A. Roy-Chowdhury, Molecular Plant **4**, 922–931 (2011).
[10] A. Medyukhina, T. Meyer, S. Heuke, N. Vogler, B. Dietzek, and J. Popp, Applied Optics **52**, 6979–6994 (2013).
[11] M. Liu, and P. Xiang, Pattern Recognition, (Springer, 2014), pp. 382–391.
[12] E. Glory, and R. F. Murphy, Developmental Cell **12**, 7–16 (2007).
[13] Q. Li, X. Zhou, Z. Deng, M. Baron, M. Teylan, Y. Kim, and S. T. Wong, Biomedical Imaging: From Nano to Macro, 2009. ISBI'09. IEEE International Symposium (2009), pp. 1255–1258.
[14] K. Mkrtchyan, A. Chakraborty, and A. K. Roy-Chowdhury, Biomedical Imaging (ISBI), IEEE 10th International Symposium (2013), pp. 672–675.
[15] T. Cervinka, Tampereen Teknillinen Yliopisto. Julkaisu-Tampere University of Technology. Publication; (2014), p. 1236.
[16] H. Hu, G. Chen, Y. Liu, and P. Wang, Image and Signal Processing (CISP), 6th International Congress (2013), pp. 588–592.
[17] O. Dzyubachyk, W. Van Cappellen, J. Essers, W. J. Niessen, and E. Meijering, Medical Imaging, IEEE Transactions on **29**, 852–867 (2010).
[18] E. Decenciere, E. Tancrède-Bohin, P. Dokládal, S. Koudoro, A. M. Pena, and T. Baldeweck, Skin Research and Technology **19**, 115–124 (2013).
[19] D. A. Dombeck, A. N. Khabbaz, F. Collman, T. L. Adelman, and D. W. Tank, Neuron **56**, 43–57 (2007).
[20] J. Wang, and X. Wang, Pattern Analysis and Machine Intelligence, IEEE Transactions on **34**, 1241–1247 (2012).
[21] A. Levinshtein, A. Stere, K. N. Kutulakos, D. J. Fleet, S. J. Dickinson, and K. Siddiqi, Pattern Analysis and Machine Intelligence, IEEE Transactions on **31**, 2290–2297 (2009).
[22] C. Çiğla, Image Processing (ICIP), 2010 17th IEEE International Conference (2010), pp. 3013–3016.
[23] R. Achanta, A. Shaji, K. Smith, A. Lucchi, P. Fua, and S. Susstrunk, Pattern Analysis and Machine Intelligence, IEEE Transactions on **34**, 2274–2282 (2012).

[24] P. Kovesi, Videre: Journal of Computer Vision Research **1**, 1–26 (1999).
[25] X. Yang, H. Li, and X. Zhou, Circuits and Systems I: Regular Papers, IEEE Transactions on **53**, 2405–2414 (2006).
[26] P. Soille, Image and Vision Computing **18**, 1025–1032 (2000).
[27] G. Chen, H. Lui, and H. Zeng, Quantitative Imaging in Medicine and Surgery **5**, 17 (2015).